Proceedings of the 21st ICSMGE, Vienna, Austria, 14 – 19 June 2026. Pistrol, Adam & Schweiger (eds.)
Published by: ÖGG, Austrian Society for Geomechanics, Salzburg, Austria, ISBN 978-3-9503898-4-5
https://doi.org/10.53243/ICSMGE2026-2322

Simplified pile stress calculation method considering superstructure rocking during large earthquakes

Takehiro Okumura, Junji Hamada
R & D institute, Takenaka Corporation, Japan, okumura.takehiro@takenaka.co.jp

ABSTRACT: During large earthquakes, the bending moment and shear force in piles are determined by the following three factors: inertial force (or pile-head horizontal displacement), pile-head moment (or pile-head rotation), and ground deformation. In Japanese structural design, both the inertial force and ground deformation are considered using Seismic Displacement Method analysis. The analysis that excludes pile head rotation leads to an overestimation of the pile head stress, which results in a conservative design. Incorporating pile head rotation into the analysis enables a more economical design. However, this method requires accurate pile head rotation calculations. This study presents dynamic centrifuge model tests in a 50 g field using models considering soft clayey ground and a superstructure model with a large moment of inertia. Based on the centrifuge model test results, we proposed a simplified pile stress calculation method that considers the superstructure rocking motion. The calculation method involves two steps: response analysis of the superstructure and stress analysis of the piles. The response analysis model has one mass and two degrees of freedom: superstructure vibration and rocking. It is calculated using only five parameters: the equivalent weight of the superstructure, natural period of the superstructure's vibration and rocking, and their respective damping factors. The pile stress calculation method was derived from the theoretical calculation method with the addition of pile head rotation. By comparing the test and analysis results, it was found that the measured vertical stiffness at the pile head was lower than the theoretical value because the tensioned pile caused both a reduced confining pressure around the pile and a decrease in ground shear stiffness. The response analysis using the experimental vertical stiffness of the pile accurately reproduced the acceleration of the superstructure and rotation angle of the foundation. In addition, the estimated bending moment of the piles closely matched the experimental results.

KEYWORDS: Pile foundation, earthquake, superstructure rocking

1 INTRODUCTION

The stress generated in piles during a large earthquake is determined by the pile head inertial force (or displacement), pile head rotational moment (or rotation angle), and the ground displacement. In the seismic displacement method used for calculating pile stress in Japanese building design, mainly pile head inertial force and ground displacement are used, and it is common practice to fix the pile head rotation (rotation angle 0) to evaluate stress conservatively for a safe design (AIJ, 2019). However, three factors contribute to the pile-head rotation during earthquakes. These include 1) the rotation due to the deformation of foundation beams connecting piles, 2) the rotation due to mechanisms that promote pile head rotation (the so-called semi-rigid pile head connection method), and 3) the rotation due to the rotational movement of the superstructure (the so-called superstructure rocking motion). The effect of foundation beam rigidity on pile head rotation has been studied in the previous study (Kimura et al. , 2007). The effect of the semi-rigid pile head connection method on pile head rotation was considered in previous study (Hamada et al., 2013). The authors focused on the effect of superstructure rocking motion on pile head rotation and conducted several centrifuge experiments simulating a plate-shaped building on soft clay ground, where the rotational angle due to rocking motion and ground displacement were observed. The results revealed that when a building has a large moment of inertia, the peak times of the inertial force and overturning moment differ from each other (Okumura et al., 2021; Okumura & Hamada, 2022). In the case of piled-raft foundations, where the influence of pile head rotation becomes significant, bending moments causing compression at the pile head displacement direction end occur owing to rotation angles exceeding free-head conditions, contrary to the typical tension that would be expected (Okumura & Hamada, 2025). These findings indicate that considering pile head rotation could potentially rationalize the current design methods while also posing risks, highlighting the importance of accurately evaluating pile head rotation to understand the pile stress during earthquakes.

This study proposes a simple response analysis method for calculating the pile head rotation angle owing to superstructure rocking and a method for calculating the pile stress by considering the pile head rotation. Additionally, we report the results of the verification by comparing the calculation results obtained using this method with the centrifuge model experiment results.

2 CENTRIFUGE EXPERIMENT

2.1 *Centrifuge model*

Figure 1 shows the prototype of a building with a pile foundation. Figures 2 and 3 show schematic diagrams of the centrifuge models (in a 50 g field). A prototype of the building model was assumed to be a plate-shaped building (13 stories, 40.0 m height, and a first natural period of 0.412 s). The dimensions of the building in the long and short directions are 12.0 m and 6.0 m, respectively. In the superstructure modeling, the two models, Case 1-2 and Case 3-1 were prepared. For Case 1-2, the weight and first to third natural periods were combined with the prototype according to the similarity law in a 50 g centrifugal field (Kazama & Inatomi, 1993) as a three-layer frame structure based on the eigenvalue analysis under the fixed pile head condition. For Case 3-1, the weight, first natural period, and moment of inertia were combined with the prototype as a single-layer truss structure. As a result, the reaction force of Case3-1 turned out to be twice as large as that of Case 1-2 in the horizontal loading analysis under the condition of the fixed foundation in Case 3-1. The piles were modeled after a cast-in-place concrete belled pile (with a shaft diameter of φ 1.5 m and a bell diameter of φ 2.2 m) using aluminum pipes (30 mm in diameter and 1.5 mm in thickness), and aluminum alloy was used for their tips. As shown in Figure 2, accelerometers, displacement transducers, piezometers, and strain gauges were installed to measure the seismic behavior, pile stress, and pore water pressure. The model ground comprised two layers: a load-bearing layer and a clayey layer. Iide silica sand No. 4 (relative density D_r = 90%) with 100 kg/m^3 of cement (W/C = 100%) was used as the load-

bearing layer, which was strong (unconfined compression strength q_u = 1.4 N/mm^2) and stiff (shear wave velocity V_s = approximately 550 m/s). The clayey layer was a reconstructed sample of Kanto loam collected in Tokyo, Japan. The clayey layer was prepared by wet compaction at an optimum water content (w = 63.1%) to achieve the maximum dry density (ρ_d = 0.943 g/cm^3) to facilitate consolidation in the centrifuge. Because the sand content was over 30%, it became nonplastic (NP) in the consistency test. Water was used for the pore fluid because the permeability of the Kanto loam is very low at 9.0 x 10^{-5} cm/s. Thus, we consider that the effect of drainage during shaking is sufficiently small. The detailed soil properties are described in a previous study (Okumura & Hamada, 2022).

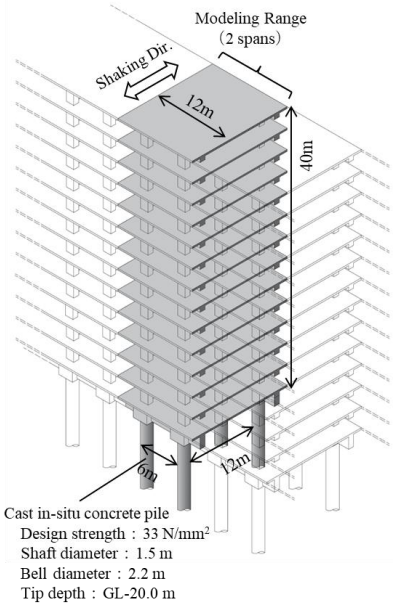

Figure 1. Schematic diagram of the prototype plate-shaped building for the superstructure and pile models.

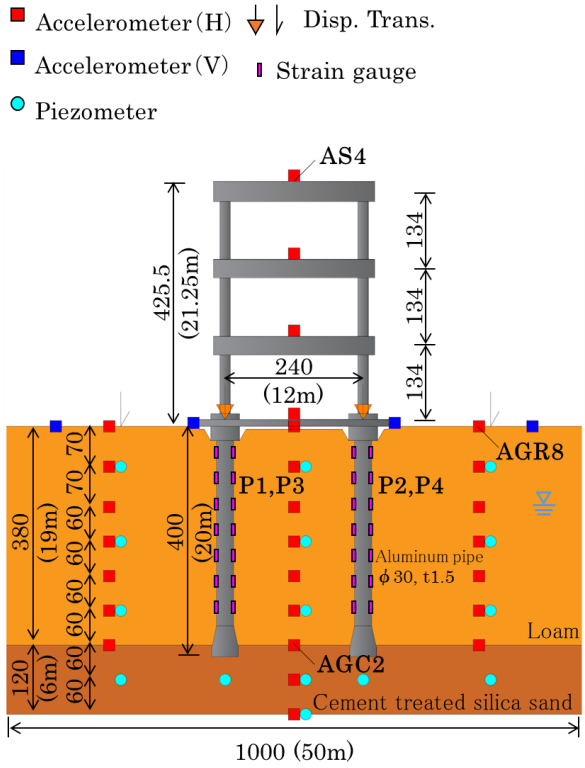

Figure 2. Schematic of the centrifuge model (Case1-2).

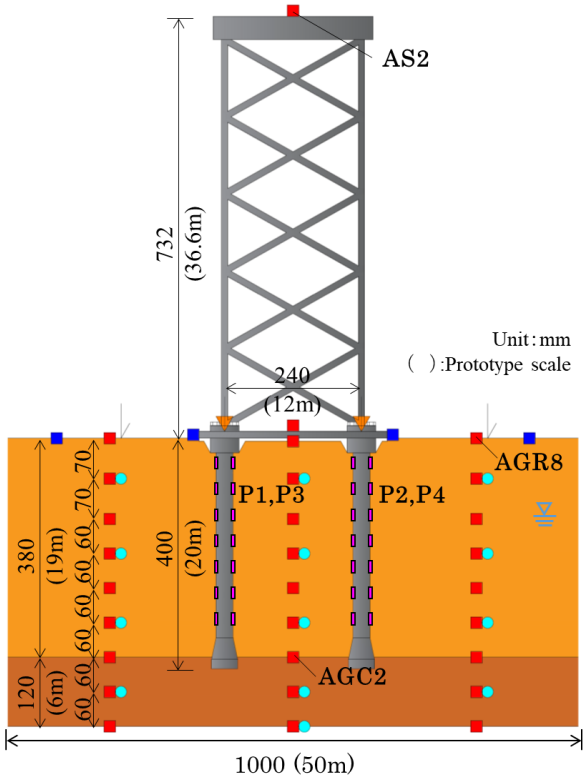

b) Case3-1

Figure 3. Schematic of the centrifuge model (Case3-1).

2.2 *Input motion*

The shaking table tests were conducted after confirming that the surface settlement of the loam layer and pore water pressure had stabilized. Figure 4 shows an example of the input seismic motion. The input motions used in the shaking table tests were the within motions (E+F) of Notification L2 with the Kobe phase (BSLJ, 2000; Okumura & Hamada, 2022), with waveforms having maximum accelerations of 0.5 to 6.0 m/s^2 in outcrop motion (2E), applied sequentially. Table 1 shows the relationship between 2E and E+F. In this study, to examine the effects of inertial force and pile head rotation on pile stress among the influences of inertial force, pile head rotation, and ground deformation, we used the results of vibration experiments with relatively small accelerations of up to 2.0 m/s^2 in 2E equivalent.

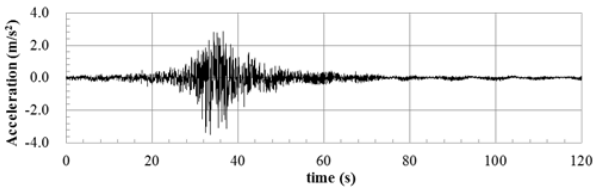

Figure 4. Input motion (2E).

Table 1. Peak acceleration used in the shaking table tests.

Case Number	Peak acceleration (m/s^2) Outcrop (2E)	Within (E + F)
0	(30–200 Hz Sweep wave)	
1	0.50	0.35
2	2.00	1.23
3	3.50	2.14
4	4.50	2.96
5	6.00	3.85
6	0.50	0.35

3 SIMPLIFIED RESPONSE ANALYSIS WITH SUPERSTRUCTURE ROCKING MOTION

The analytical model is illustrated in Figure 5. The analytical model is a single-mass model with two degrees of freedom: the displacement of the superstructure vibration x_b and the superstructure rocking angle θ.

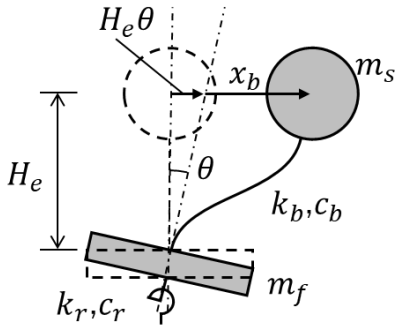

Figure 5. Schematic of the simplified response analysis model.

For this model, the acceleration of the superstructure $\ddot{x}_b$ and the rotational acceleration of the superstructure $\ddot{\theta}$ with respect to the effective input acceleration $\ddot{y}_f$ (acceleration of the foundation) are expressed in the frequency domain as follows:

$$\begin{Bmatrix} \ddot{X}_b \\ H_e\ddot{\theta} \end{Bmatrix} = -\boldsymbol{A}^{-1}\begin{Bmatrix} 1 \\ 1 \end{Bmatrix}\ddot{Y}_f \tag{1}$$

$$\boldsymbol{A} = \begin{bmatrix} 1 - \dfrac{ic_b}{m_s\omega} - \dfrac{k_b}{m_s\omega^2} & 1 \\ 1 & 1 - \dfrac{ic_r}{m_sH_e^2\omega} - \dfrac{k_r}{m_sH_e^2\omega^2} \end{bmatrix} \tag{2}$$

Here, the uppercase of $\ddot{x}_b$, $\ddot{\theta}$, $\ddot{y}_f$ represents their Fourier transforms, and i and ω are the imaginary unit and angular frequency, respectively. In addition, k_b and c_b are the stiffness and damping coefficient for the vibration of the superstructure, respectively. In addition, k_r and c_r are the superstructure rocking motion's ones. Next, p_b and p_r are the natural angular frequencies related to the superstructure vibration and rocking, respectively, and are expressed by the following equations using the natural period of the superstructure's vibration T_b and rocking T_r:

$$p_b = \frac{2\pi}{T_b} = \sqrt{\frac{k_b}{m_s}} \tag{3}$$

$$p_r = \frac{2\pi}{T_r} = \sqrt{\frac{k_r}{I_m}} = \sqrt{\frac{k_r}{m_sH_e^2}} \tag{4}$$

Using p_b and p_r, Equation 5 can be obtained from Equation 2.

$$\boldsymbol{A} = \begin{bmatrix} 1 - 2ih_b\dfrac{p_b}{\omega} - \left(\dfrac{p_b}{\omega}\right)^2 & 1 \\ 1 & 1 - 2ih_r\dfrac{p_r}{\omega} - \left(\dfrac{p_r}{\omega}\right)^2 \end{bmatrix} \tag{5}$$

According to Equations 1 to 5, the response of the superstructure, including rocking, can be calculated from only five parameters: the time history of the input acceleration (effective input motion of the foundation) $\ddot{y}_f$, the equivalent height of the superstructure mass H_e, the natural period T_b and the damping constant h_b related to the superstructure vibration, and the natural period T_r and the damping constant h_r related to superstructure rocking. Tables 2 and 3 show the calculation parameters (prototype scale) used in the reproduction analysis of the above experiment. The masses of the superstructure and foundation, m_s and m_f, respectively, are the measured values of the model, and the moment of inertia I_m is the sum of each mass multiplied by the square of the center height. The equivalent height H_e of the mass in the analytical model was calculated to match the moment of inertia of the model. T_b is the design value of the model, and T_r is determined from Equation 4 using the moment of inertia I_m and the rotational stiffness of the pile foundation K_r.

Table 2. Parameters of the response analysis.

Case			1-2	3-1
Superstructure's Mass	m_s	(Mg)	3,111	2,418
Foundation's Mass	m_f	(Mg)	792	1,447
Moment of Inertia	I_m	(Ggm^2)	656	3,013
Equivalent Mass Height	H_e	(m)	14.5	35.3
Superstructure's Vibration (Cal.)	T_b	(s)	0.412	0.412
	h_b		0.02	0.02
Superstructure's Rocking (Exp.)	T_r	(s)	0.427	0.915
	h_r		0.02	0.02

Table 3. Parameters for calculating the rotational stiffness of the pile foundation K_r.

Surface ground's Vs	V_s	(m/s)	130
Surface ground's Poisson ratio	ν_e		0.4
Support Layer's Vs	V_{sb}	(m/s)	550
Support layer's Poisson ratio	ν_b		0.3
Shaft Diameter	D_p	(m)	1.5
Shaft Thickness	t_p	(m)	0.075
Tip Diameter	D_t	(m)	2.2
Pile's Length	L_p	(m)	20.0
Pile's Young Modulus	E_p	(10^4 N/mm^2)	6.86
Vertical stiffness (Cal.)	K_{vs}	(MN/m)	1,257
Rotational Stiffness (Cal.)	K_r	(GNm/rad)	180
Vertical stiffness (Exp.)	K_{vs}	(MN/m)	972
Rotational Stiffness (Exp.)	K_r	(GNm/rad)	140

The rotational stiffness K_r is determined as follows (AIJ, 2006): First, the vertical springs at the pile head are divided into pile-soil springs and pile tip springs. The pile-soil spring S_v is the pile peripheral spring according to Randolf and Wroth (1978), and is determined by the following equations:

$$S_v = 2\pi G_e / \log_e\left(\frac{2r_m}{D_p}\right) \tag{5}$$

$$r_m = 2.5L(1 - \nu_e) \tag{6}$$

Here, D_p: pile diameter, L: pile length to the load-bearing layer, G_e, ν_e: equivalent shear stiffness and equivalent Poisson's ratio of the surface ground. Next, the pile tip spring k_b is obtained using the following equation:

$$k_b = \frac{3\pi}{8}\frac{\pi G_b D_t}{2(1 - \nu_b)} \tag{7}$$

Here, D_t: tip diameter, G_b, ν_b: shear modulus and Poisson's ratio of the bearing layer. As described above, the vertical spring

constant at the pile head K_{vs} can be obtained from the following equation using the calculated pile shaft spring S_v and pile tip spring k_b.

$$K_{vs} = E_pA_p\beta_s \frac{E_pA_p\beta_s(1-e^{-2\beta_sL})+k_b(1+e^{-2\beta_sL})}{E_pA_p\beta_s(1+e^{-2\beta_sL})+k_b(1-e^{-2\beta_sL})} \quad (8)$$

Here, $\beta_s^2 = S_v / E_pA_p$, where E_p is the Young's modulus of the pile and A_p is the cross-sectional area of the pile. Finally, the rotational spring of the pile foundation K_r is obtained by summing the pile head springs multiplied by the square of the distance xi from the center of rotation, as follows:

$$K_r = \sum K_{vs}x_i^2 \quad (9)$$

The amplification ratios of the superstructure mass against the input motion at the foundation in the analytical model calculated using the parameters obtained from the above tables are shown by the blue lines in Figure 6, while the amplification ratio of the top of the superstructure against the foundation in the experiments is shown by the black lines in the same figure. The natural period inferred from the maximum value of the amplification ratio was smaller in the calculated value than in the experiment, suggesting that the natural period of the superstructure's vibration or the natural period of rocking was larger than the calculated value.

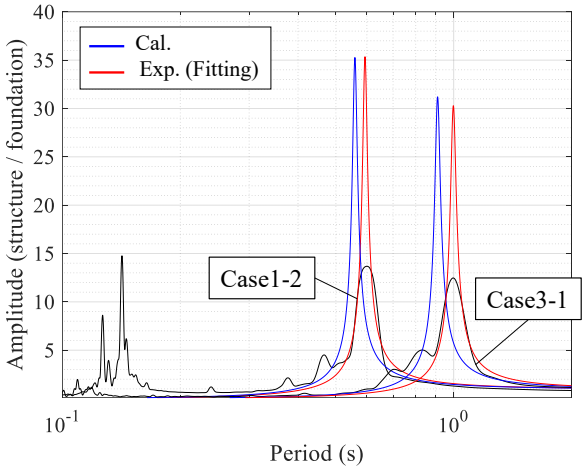

Figure 6. Transfer function of structure top against foundation

Therefore, the relationship between the pile head displacement and the variation of the axial force for each pile are shown in Figure 7. The variation in the axial force was obtained by cubic spline interpolation of the axial forces measured by the strain gauges at each depth, extrapolated to the GL-0 m for each time point. The pile-head stiffness K_{vs} calculated using the above equation is also shown by the blue line in the same figure. The results of Case 1-2 are shown in Figure 7a), the slope on the compression side of the experiment generally matches K_{vs}, but the slope on the tension side is slightly smaller than the K_{vs} slope. However, for Case 3-1 shown in Figure 7b), compared to the Case 1-2 data, there are scattered plots, and a less-matched trend can be observed than in Case 1-2, but the slope is generally smaller than K_{vs}. A possible reason for these results is that when the pile was pulled, the confining pressure of the soil around the pile decreased, which reduced the shear stiffness of the soil. Next, the pile-head stiffness K_{vs} was determined, as shown in Table 3, to be consistent with the experimental result trends in Figures 6 and 7. The theoretical amplification ratio and slope based on this are shown by the red lines in Figures 6 and 7. The rocking natural period T_r obtained from the foundation rotational spring K_r derived from this experimental K_{vs} was set as shown in Table 3 and used in subsequent investigations.

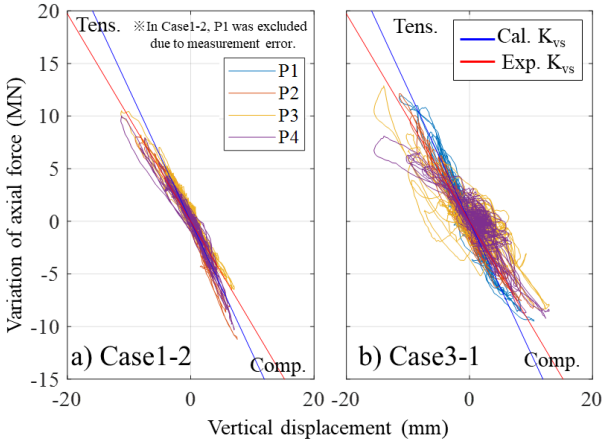

Figure 7. Relationship between vertical displacement of pile heads and variation in axial force.

4 CALCULATION METHOD OF PILE STRESS

The pile stress is calculated from the response acceleration ($\ddot{x}_b$, $\ddot{\theta}$) obtained by the above analytical method. The rotation angle $\theta(t)$ in the following equations is positive in the counterclockwise direction, which differs from that in Figure 5. First, as shown in Equation 10, the time history of the inertial force of the entire structure $H(t)$ is calculated by multiplying the response acceleration of the superstructure and the acceleration of the foundation by the masses of the superstructure and foundation, respectively.

$$H(t) = -m_s(\ddot{x}_b + H\ddot{\theta} + \ddot{y}_f) - m_f\ddot{y}_f \quad (10)$$

Next, to make the displacement at the top of each pile the same, the displacement of the foundation $y(t)$ is determined using the following equation:

$$y(t) = \frac{H(t) - \sum 2EI\beta^2\,\theta(t)}{\sum 4EI\beta^3} \quad (11)$$

Here, β ($= \sqrt[4]{k_hD_p/4E_pI_p}$) is the characteristic value of the pile, and the coefficient of subgrade reaction k_h is calculated according to the following equations (AIJ, 2019): E_p, I_p, and D_p are the Young's modulus, moment of inertia of the cross-section, and the diameter of the pile, respectively.

$$k_{h0} = 80E_0(D_p/0.01)^{-3/4} \quad (12)$$

$$E_0 = E_{ps}/30 = 2(1+\nu_e)\rho V_s^2/30 \quad (13)$$

$$k_h = \alpha k_{h0} \quad (14)$$

The shear wave velocity V_s of the surface ground was set to 130 m/s for Case 1-2 and 100 m/s for Case 3-1, based on the transfer function of the ground. Additionally, the coefficient α in Equation 14, which is used for the relative displacement between the pile and ground, typically takes values below 3.16 ($= \sqrt{10}$), but in this study, it was set to 3.16. Using the obtained foundation displacement $y(t)$ and superstructure rocking angle $\theta(t)$, the bending moment and shear force of the pile at depth z from the pile head can be calculated using the following equations:

$$M(z,t) = 2EI\beta^2e^{-\beta z}\{(y(t)+\frac{\theta(t)}{\beta})cos\beta z - y(t)sin\beta z\} \quad (15)$$

$$Q(z,t) = -2EI\beta^3 e^{-\beta z}\left\{\left(2y(t) + \frac{\theta(t)}{\beta}\right)cos\beta z + \frac{\theta(t)}{\beta} sin\beta z\right\} \quad (16)$$

In particular, the bending moment M_0 and shear force Q_0 at the pile head ($z = 0$) are expressed as follows:

$$M_0(t) = 2EI\beta^2\left(y(t) + \frac{\theta(t)}{\beta}\right) \quad (17)$$

$$Q_0(t) = -2EI\beta^3\left(2y(t) + \frac{\theta(t)}{\beta}\right) \quad (18)$$

As mentioned previously, the stress on the piles is further affected by ground deformation. For this calculation, methods such as those in reference (Hamada, 2019) can be used. In this study, we focused on the effects of inertial force and pile head rotation angle and conducted our investigation using inputs that caused minimal ground deformation. However, examining the impact of ground deformation on experiments with larger inputs remains a task for future research.

5 COMPARISON CALCULATION AND CENTRIFUGAL EXPERIMENT'S RESULT

The calculation results obtained using the above methods were compared with the centrifugal experimental results. The time histories of the superstructure response acceleration and rocking angle are shown in Figures 8 and 9, respectively. Note that the calculation results from a single-mass model that does not consider foundation rotation are also shown with blue lines for the response acceleration. From Figure 8, it can be confirmed that the two-degree-of-freedom model that considers superstructure's rocking reproduces the experimental results more accurately compared to the single-degree-of-freedom model that does not consider one. Additionally, the rotational angle of the rocking in Figure 9 can also be calculated with good accuracy. For the response acceleration of Case 3-1 (Figure 8b), the single-mass model showed very large accelerations with shorter periods than the experimental results. Figure 10 shows the time histories of the foundation displacement. The experimental data were calculated by second-order integration of the acceleration data observed at the foundation. In contrast, the calculation results were obtained by adding the integral result of the ground surface acceleration to Equation 11. From this figure, the proposed method can also calculate the displacement of the foundation well.

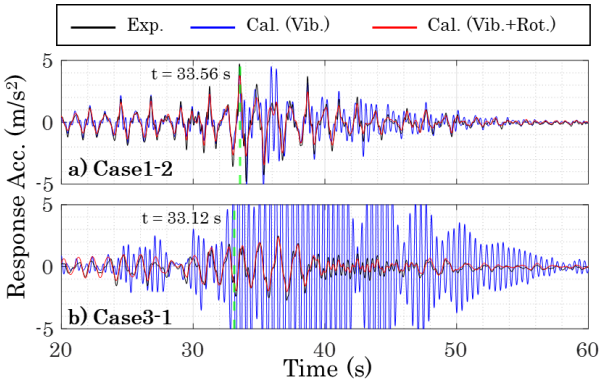

Figure 8. Time histories of the response acceleration at the top of the superstructure.

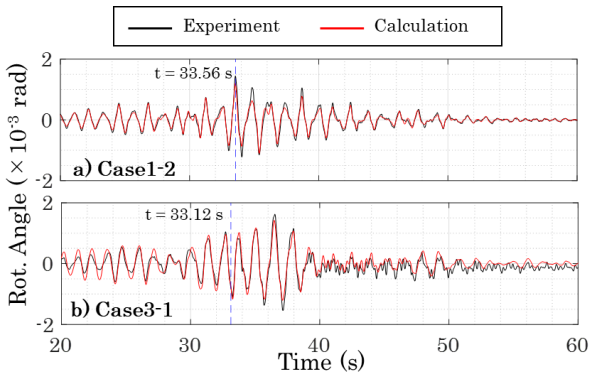

Figure 9. Time histories of the rotation angle of the foundation.

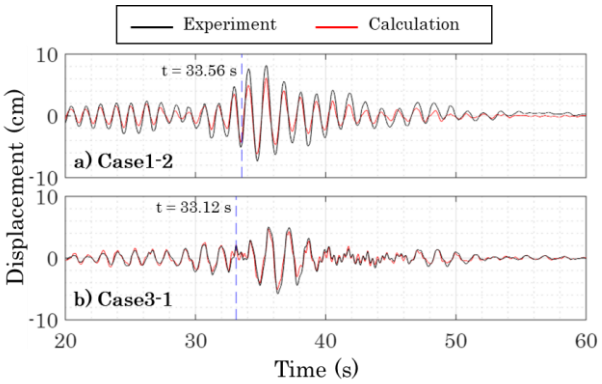

Figure 10. Time histories of the foundation displacement.

Figures 11 and 12 show the time histories of the bending moments and shear forces, respectively, from both the calculations and experiments at the strain gauge installation depth (GL-2.25m). Considering the calculated bending moments for Case 1-2 shown in Figure 11a), the calculation results with the red line well evaluate the waveform compared with the experimental results with the black line, whereas for Case 3-1 shown in Figure 11b), the amplitude of the waveform is underestimated. As a cause of this underestimation, as can be seen from Figure 10, during the time interval when the bending moment was underestimated, the foundation displacement increased, suggesting that the influence of ground deformation may have been significant. As shown in Figure 12, it can be confirmed that the shear force calculated from Equation 16 also reproduces the experimental results well. Nevertheless, despite using a simplified method, the pile stresses are reproduced with relatively good accuracy.

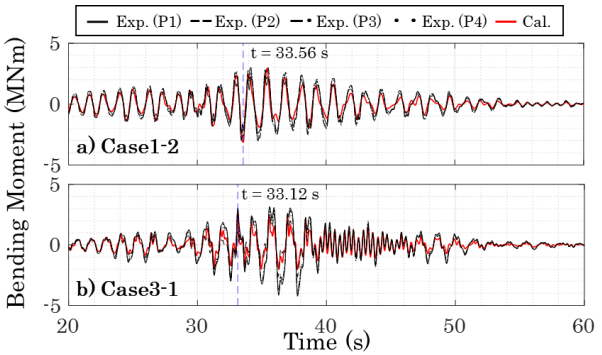

Figure 11. Time histories of the bending moment at the depth of 2.25m from the ground surface.

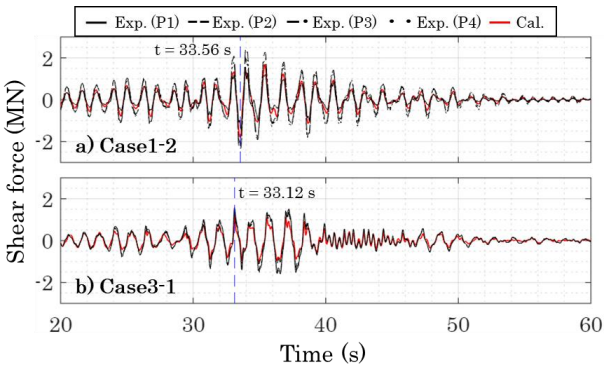

Figure 12. Time histories of the bending moment at the depth of 2.25m from the ground surface.

Figure 13 shows the depth distribution of the bending moments when the inertial force *H(t)* recorded its maximum value in each experimental case. Each plot indicates the experimental results, the solid black lines represent the bending moments calculated from Equation 15, and the black dashed lines represent the bending moments when *θ(t)* in Equations 11 and 15 is set to 0, that is with a fixed rotation at the pile head. The values of the solid lines are slightly smaller than those of the dashed lines, indicating that considering the rotation at the pile head reduces the bending moment near the pile head. This reduction in the bending moment was smaller in Case 3-1 than in Case 1-2, which was inversely proportional to the magnitude of the moment of inertia of the superstructure. As reported previously (Okumura & Hamada, 2022), this is largely attributed to the significant phase difference between the inertial force and rotation angle.

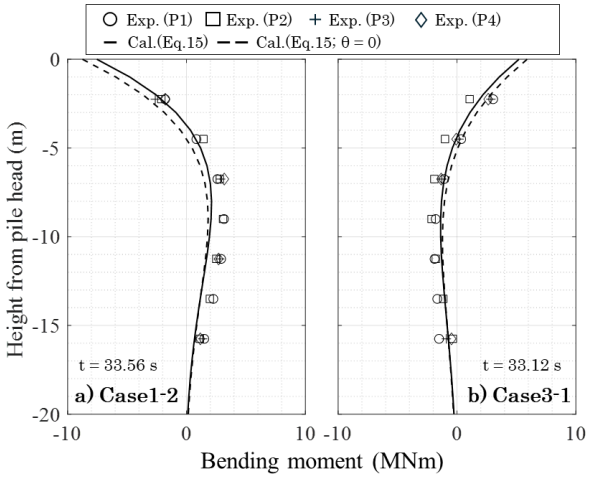

Figure 13. The bending moment profile was recorded at the time of the maximum inertial force.

6 CONCLUSIONS

In this study, we proposed a response analysis method using a single-mass system with two degrees of freedom that considers the superstructure's rocking motion to evaluate the seismic pile stress with large foundation rotation more precisely and simply. We also proposed a method to evaluate the pile stress using the response values (time history of the response acceleration and foundation rotation angle) obtained from this response analysis method. Furthermore, by comparing with the centrifugal experimental results, we obtained the following conclusions.

1. The rotational spring of the building was slightly smaller than that in the method described in reference (AIJ, 2006). Comparing the vertical springs at the pile head between the calculation and experiment, the stiffness differed between the compression and tension sides in the experiment. For piles on the tension side, the vertical spring at the pile head may decrease because the confining pressure of the soil around the pile decreases, resulting in a decrease in the shear stiffness of the soil.
2. The proposed response analysis method, although a simple approach, accurately evaluated the response acceleration of the superstructure and rotation angle of the foundation.
3. The proposed method for evaluating the pile stress successfully reproduced the time history and depth distribution of the bending moments.

As described above, we have confirmed that the proposed calculation method can calculate pile stresses during earthquakes with relatively good accuracy, considering the rocking motion of the superstructure (the rotational angle of the foundation). The effect of ground deformation, which was not addressed in this study, remains a challenge for future studies. We aim to improve the proposed calculation method by referring to existing evaluation methods for pile stresses caused by ground deformation.

7 REFERENCES

Architectural Institute of Japan, 2006. *Seismic Response Analysis and Design of Buildings Considering Dynamic Soil-Structure Interaction,* 168. (in Japanese)

Architectural Institute of Japan, 2019. *Recommendations for Design of Building Foundations*. (in Japanese)

Hamada, J., Tanikawa, T., Tsuchiya and T., Usami, T., 2013, Discussion on Estimation Methods of Pile Head Rigidity for Simplified Semi-rigid Pile Head Connection, *Journal of Structural and Construction Engineering*, 78, 688, 1095-1104. (in Japanese)

Hamada, J. 2019. Simplified Equations for Evaluation of Stresses in Piles Subjected to Ground Deformations, *Journal of Technology and Design*, 25, 59, 115-118. (in Japanese)

Japanese Ministry of Construction, 2000. *Building Standard Law of Japan: Notification 1461*. (in Japanese)

Kazama, M. and Inatomi, T. 1993. Application of Centrifuge Model Testing to Dynamic Problems, *Journal of Japan Society Civil Engineers*, 477, 83-92. (in Japanese)

Kimura, T., Syamoto, Y., Matsui, K., Mano, H., Mori, M. and Nakai, S., 2007. Effect of Foundation Girder Stiffness on Pile Response during Earthquake, *Journal of Structural and Construction Engineering*, 618, 41-48. (in Japanese)

Okumura, T., Hamada, J. and Honda, T., 2021. Study on the Seismic Behavior of the Pile Foundations Supporting a Plate-shaped Building on Clayey Ground, *Takenaka Technical Research Report*, 77.

Okumura, T. and Hamada, J. 2022. Dynamic Centrifuge Model Tests on Plate-shaped Building's Pile Foundation in the Soft Clayey Ground: Effect of Building's Moment of Inertia, *Proc. 20th International Conference on Soil Mechanics and Geotechnical Engineering*, Sydney.

Okumura, T. and Hamada, J. 2025. Effect of the Seismic Response of Superstructure on Pile's Stress of Piled-Raft Foundation Based on Centrifugal Model Tests, *Journal of Japan Association for Earthquake Engineering*, 25, 1, 200-211. (in Japanese)

Randolf, M. F. and Wroth, C. P. 1978. Analysis of Deformation of Vertically Loaded Piles, *Journal of Geotechnical Engineering Division*, 104, 12, 1465-1488.